Theory of InP nanocrystals under pressure

J. G. Díaz and Garnett W. Bryant*
National Institute of Standards and Technology, 100 Bureau Drive, Stop 8423, Gaithersburg, Maryland 20899-8423, USA

W. Jaskólski and M. Zieliński†
Instytut Fizyki UMK, Grudziądzka 5, 87-100 Toruń, Poland

(Received 30 January 2007; revised manuscript received 4 May 2007; published 27 June 2007)

An empirical tight-binding theory which includes the effects of lattice relaxation is employed to investigate the optoelectronic properties of InP nanocrystals under external hydrostatic pressure. For bulk InP, our model accurately describes the evolution of the lowest conduction-band edges with pressure and predicts the Γ_{1c}-X_{1c} crossover at the same lattice contraction as measured in experiment. For small InP nanocrystals, the lattice-relaxed tight-binding model is compared with a tight-binding model which assumes a scaled bulklike arrangement for the atoms in the nanocrystal. Atomistic bond-length-scaling models predict that a direct-to-indirect band gap (the Γ_{1c}-X_{1c} crossing) produces the redshift observed experimentally in nanocrystals at high pressure. However, the scaling models are not able to describe quantitatively the band-gap evolution with pressure. When lattice relaxation effects are included, the band-gap dependence on pressure agrees quantitatively with the experimental results. The agreement in the band-gap variation with pressure is due to the stronger mixture between Γ_{1c} and L_{1c} minima and the more localized character of hole states. Moreover, in the lattice-relaxed model, the experimental redshift results as a transition of the lowest states from bound states localized inside the dot to surfacelike states on the dot exterior, rather than as the direct-to-indirect band gap crossover.

DOI: 10.1103/PhysRevB.75.245433 PACS number(s): 78.67.Bf, 73.22.Dj

I. INTRODUCTION

External hydrostatic pressure can be applied to modify both the chemical and the physical properties of semiconductor crystals. Thus, II-VI and III-V covalent zinc blende semiconductors can undergo phase transitions to either the ionic rocksalt and/or the white-tin (β-Sn) structures.[1,2] For example, bulk InP transforms from zinc blende to rocksalt structures at $\approx$11 GPa,[3] whereas a set of zinc blende/rocksalt/β-Sn transitions has been observed for bulk InAs.[4] *Structural* phase transitions usually take place at high pressures. Lower hydrostatic pressures can be employed to modify the *electronic* and *optical* properties of zinc blende semiconductors. Direct ($\Gamma_{1c} \leftarrow \Gamma_{1v}$) and indirect $X_{1c} \leftarrow \Gamma_{1v}$ transitions respond differently under applied pressure. The Γ_{1c} energy increases when pressure is applied, while the X_{1c} energy decreases. This is a direct consequence of the different character for the conduction-band (CB) edges (*bonding like* at the X_{1c} edge and *antibonding* at the Γ_{1c} edge[5]) that yields opposite signs for the Γ_{1c} and X_{1c} deformation potentials on a reduction of the lattice constant. Thus, for direct-gap semiconductors such as CdSe or InAs, an increasing pressure gives rise to a larger band gap. However, in bulk semiconductors such as GaAs or InP, where the X_{1c} minima are not too far above the Γ_{1c} edge, a crossover from direct to indirect gap behavior can be observed, e.g., at $\approx$4 GPa for GaAs (Ref. 6) and $\approx$11 GPa for InP (Ref. 7), leading to a reduction of the band gap after the crossover.

In nanocrystals, the three-dimensional confinement transforms the bulk band structure into a series of discrete energy levels. These discrete states behave similarly with pressure as the corresponding bulk-band valleys from which they arise. This similarity provides the intuition about how the nanocrystal electronic structure changes under pressure. Because the Γ_{1c} edge has a lower effective mass than the surface edge points (X_{1c} and L_{1c}), the Γ_{1c}-derived energy states increase much faster with confinement than the L_{1c} and X_{1c} states. For GaAs nanocrystals, confinement itself is enough to cause the direct-to-indirect crossover because the lowest bulk CB edges are close enough in energy. The indirect-gap behavior has been observed for GaAs dots with sizes below 2.5 nm (Ref. 8) and confirmed by the calculations performed with the tight-binding approach.[9] In contrast, for InP nanocrystals, confinement alone is not sufficient to induce the direct-to-indirect crossover at atmospheric pressure.[10] However, in nanocrystals, confinement can reduce the X_{1c}-Γ_{1c} and L_{1c}-Γ_{1c} energy separations significantly compared to the bulk separations. Thus, a lower pressure should be required to induce an electronic crossover. Moreover, confinement usually causes pressure-induced structural phase transitions to occur at higher pressures relative to the bulk transition.[11] Therefore, the indirect-band-gap crossover, that is obscured in bulk InP because it occurs at a similar pressure as the phase change from zinc blende to rocksalt structures,[3] could be investigated in the quantum confinement regime without being obscured by the structural phase transition.

Menoni *et al.* studied the photoluminescence (PL) as a function of pressure for InP nanocrystals with mean diameters $\langle D \rangle = 32$ and 35 Å.[12] For clarity, the band-gap evolution with pressure has been classified into four different regions, as shown schematically in Fig. 1. In region 1 (0–2 GPa), we observe a linear increase of the band gap with pressure. For larger pressures (region 2, 2–6 GPa), a bowing in the band-gap evolution occurs. In regions 1 and 2, the band gap blueshifts. However, at about 7 GPa a downturn appears (region 3). The transition occurs well below the bulk transition at 11 GPa. The downturn leads to a region where the band gap decreases with the increasing pressure (region 4). The band-

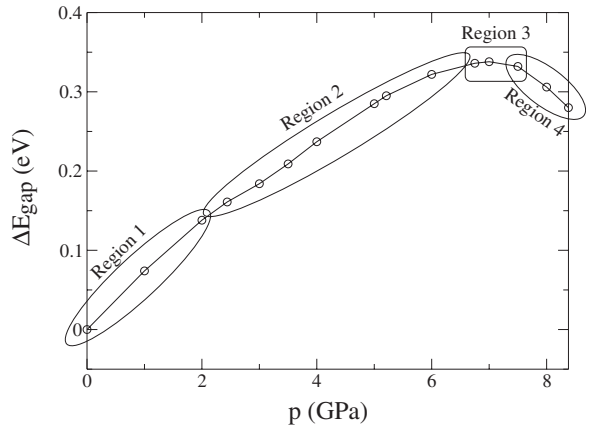

FIG. 1. Schematics for the band-gap evolution with pressure. Four different regions can be distinguished: region 1 (0–2 GPa), the band gap varies linearly with pressure; region 2 (2–6 GPa), nonlinear dependence with pressure; region 3 (≈7 GPa), the downturn; and region 4 ($p>7$ GPa), the band gap redshifts.

gap downturn was attributed to the existence of a Γ_{1c}-X_{1c} crossover. However, the mechanism of the crossover was not fully understood.[12] The pressure-induced downturn in small InP nanocrystals was also investigated by Lee *et al.*[13] Contrary to expectations, Lee *et al.* observed little reduction of the transition pressure in nanocrystals as compared to the bulk.

In this paper, we employ empirical tight-binding (TB) theory to study the optical properties of InP nanocrystals under hydrostatic pressure. A ten-orbital $sp^3d^5s^*$ basis set has been used to describe each atom in the nanocrystal. Spin-orbit coupling is also included. This TB model can accurately describe the optical properties of both III-V (Refs. 9 and 14) and II-VI (Ref. 15) homogeneous nanocrystals and strained multishell structures with the shell thickness down to a single monolayer.[16] The inclusion of d orbitals in the basis set is necessary for a proper description of the effective masses at the conduction-band edges X_{1c} and L_{1c}.[17] To confirm that this TB model should work well for InP nanocrystals, we study the evolution with pressure for the lowest bulk InP CB edges and, in particular, the Γ_{1c}-X_{1c} crossover. The bulk predictions arising from our TB model are compared with bulk experimental results (Refs. 7, 18, and 19).

We employ two different approaches to describe how pressure affects the nanocrystal. In the first model, we assume that hydrostatic pressure leads to a homogeneous scaling of the bond lengths for the whole nanocrystal. This approach was employed previously in the framework of pseudopotential theory[5] and the Wannier function method.[20] In the second model, the atoms in the nanocrystal are allowed to relax in the given volume determined by the pressure applied. Once the structure is defined in either model, the bulk TB model is adjusted to account for changes in bond lengths and angles. The pressure dependence of the lowest electron and hole levels of nanocrystals with different sizes is analyzed in detail within these two TB models. Particular attention is paid to the role of the L_{1c}-derived states in the vicinity of the downturn. We show that the response of the ground electron and hole levels as a function of pressure is different for the two TB models. Different mechanisms are suggested by the two models to explain the band-gap downturn observed experimentally. To test the reliability of our models, we compare the predicted band-gap evolution with pressure and the predicted intensity of the emission peak with photoluminescence experiments.[12,13]

The influence of nanocrystal size, geometry, and degree of surface passivation is addressed within the two TB models to check the dependence of our results on experimental uncertainties. Synthesized InP nanocrystals exhibit a degree of ellipticity.[21] The role of the geometry distortions away from a spherical shape is considered in this work. The effect of the partial passivation of surface atoms is modeled to better understand why the nanocrystals in Ref. 13 exhibit a downturn at pressures similar to the bulk downturn. In addition, we study the near-band-edge absorption spectra to describe the changes in optical properties of InP nanocrystals as a function of pressure.

II. THEORY AND COMPUTATIONAL DETAILS

In our TB calculations, we assume that the atoms in an unrelaxed InP dot are located on a zinc blende lattice. The zinc blende structure is inferred from experimental powder x-ray diffraction patterns.[21,22] A ten-state atomiclike (s; x, y, z; s^*; xy, yz, zx, x^2-y^2, $3z^2-r^2$) basis set is used to describe each atom in the nanostructure. Interactions are restricted to nearest neighbors only. The inclusion of d orbitals into the minimal basis set is necessary to provide a correct description of the bulk-band dispersions at high symmetry points at the edge of the Brillouin zone.[17] Simpler sp^3s^* TB models yield an incorrect description of electron states made from bulk bands away from the Brillouin zone center and cannot be employed to accurately describe the indirect-gap behavior, as was shown previously for small GaAs nanocrystals.[9] Spin-orbit interactions were described in the $sp^3s^*d^5$ model by including only the contribution from p states. The much smaller splittings of excited d states were neglected. This gives rise to a model with 29 different empirical parameters that were obtained from Ref. 17. Unless otherwise stated, we passivate surface dangling bonds to push dangling-bond-derived surface states out of the band gap. This is achieved by shifting the energies of sp^3 hybridized dangling bond orbitals on surface atoms by a high added potential.[23] When a smaller added potential is used, the surface states due to dangling bonds lie closer to the band gap. Level repulsion between the surface states and the interior states can occur. Anion-centered dots are considered here. Test calculations for cation-centered and midbond-centered dots give similar results.

The importance of surface relaxation and the role of ligands on the surface relaxation of nanocrystals have been studied with the tight-binding model, in particular, for CdSe nanocrystals at zero pressure.[24,25] Surface relaxation at zero pressure provides a few percent bond change at the surface and a significantly smaller bond change inside the dot. Thus, it is a smaller bond-length change than the bond-length changes we find at higher pressures. For CdSe, the metal surface atoms move in toward the center of the dot, while the

Se surface atoms move only slightly outward.[24] Passivation by organic ligands reduces the displacement of the metal atoms. Thus, these effects tend to cancel and, in any case, are typically smaller than the bond distortions that we find, especially at higher pressures. In this paper, we ignore the effects of any surface relaxation that would arise at zero pressure.

In many of the successful atomistic nanocrystal calculations to date, lattice and surface relaxation have been ignored completely. However, recently we also showed that lattice relaxation due to interface lattice mismatch in core-shell nanocrystals can have critical effects.[16] A key point of the present paper is that lattice relaxation is important in a homogeneous dot when pressure is used to distort the lattice away from the bulk configuration. We will focus here on the effects of the lattice relaxation induced by the pressure and leave unresolved the question of how important the contribution of any additional weak zero-pressure surface relaxation might be.

In the bond-length-scaling model, hydrostatic pressure is assumed to reduce homogeneously the bond lengths for the whole nanocrystal without altering the bond angles. The nanocrystal retains the perfect zinc blende structure, but with bond lengths reduced from the bulk value. A power-law scaling is used to modify the off-site TB parameters, V_{lm}, due to the contracted bond lengths: $V_{lm}=V_{lm}^0\left(\frac{d_{ij}^0}{d_{ij}}\right)^{\kappa_{lm}}$, where d_{ij} is the bond length between the nearest neighbors i and j and the superscript 0 corresponds to the bulk values. The exponents κ_{lm} for the different off-site TB parameters are determined by fitting the InP volume deformation potentials under hydrostatic pressure to their experimental values.[17] The effect of pressure can be measured in terms of the lattice constant contraction $\Delta a/a_0$, where a_0 is the bulk lattice constant with no pressure applied.[5,13] Lattice compression can be related to pressure p via Murnaghan's equation:[26] $p=\left(\frac{B_0}{B_0'}\right)\left[\left(\frac{a_0}{a}\right)^{3B_0'}-1\right]$, where B_0 is the bulk modulus [$B_0=76\pm4$ GPa (Ref. 3)] and B_0' is its derivative with respect to pressure [$B_0'=4\pm0.2$ (Ref. 3)].

In the lattice-relaxed model, the valence force field method is used to minimize the strain energy in a nanocrystal under hydrostatic pressure. To start the relaxation, the atoms in the dot are located on a regular zinc blende structure with a uniform and very small bond length. This arrangement leads to an enormous strain because the atoms are far from their bulk positions. We assume spherical boundary conditions for the lattice relaxation: atoms in the dot are allowed to expand in a sphere of a volume that is determined from the external hydrostatic pressure applied. The only restriction for the free movement of the atoms in any direction is that they cannot exceed the cut-off radius for the volume.[27] Any atom that, in the process of relaxation, goes beyond the cut-off radius is pushed back to the spherical volume by setting to zero the radial strain force on that atom. The minimization of the strain energy is performed using the conjugate gradient technique.[28] The relaxation of the lattice leads to new atomic positions where not only bond lengths but also bond angles vary in the nanocrystal. This gives rise to different TB matrix elements between neighboring atoms. To incorporate the effects of changed bond angles on the Hamiltonian, we employ the Slater-Koster formulas.[29] Pressure can be estimated by calculating the force applied on surface atoms to compress the nanocrystal from the bulk configuration. Effectively, the force due to the applied pressure balances the radial force due to strain. The lattice-relaxed model and the scaling model are compared for nanocrystals with the same average bond length. The pressure calculated from the force applied on surface atoms agrees with the pressure obtained employing the average bond length in Murnaghan's equation.

Once the nanocrystal structure is defined, the electron and hole eigenvalues are found by diagonalizing the TB Hamiltonian by means of an iterative solver. We estimate the energies of optical transitions by the differences between the energies of the electron and hole states. Coulomb energy can be estimated by the formula $E_C=1.786\frac{e^2}{\epsilon R}$, where e is the charge of the electron, ϵ is the dielectric constant of the material, and R is the nanocrystal radius, and subtracted from the single-particle transitions to estimate the exciton energy. In the context of the tight-binding model and for other atomistic approaches, more complete calculations of excitonic effects are typically done using configuration interaction approaches. These more complete calculations are needed to get the best estimate of the absolute position of the band gap and to describe excitonic fine structure near the band gap. Here, we are interested in the shift of the band gap with pressure. Over the range of pressures considered, the single-particle band gap changes by 400 meV or more. Over the same range, the lattice constant is reduced by 5%. This leads to a Coulomb energy increase of 5%. At zero pressure, the Coulomb energy should be on the order of 100 meV. Thus, any changes in the Coulomb energy due to pressure should be about 1% of the changes in the single-particle energies. Thus, the simple model for the Coulomb energies should suffice here. Excitonic effects are most important for mixing closely spaced hole levels. This mixing is not included here because we do not focus on the excitonic fine structure. The crossing of the electron bands is the effect that influences most the transition pressure. Away from the transition point, these states are widely spaced and are not strongly mixed by excitonic effects. It is only very near the transition point that excitonic mixing could compete with the band crossings due to pressure. Again, we expect the simple model for Coulomb effects to suffice here. TB oscillator strengths are calculated by evaluating the dipole matrix elements using the electron and hole states. The nonzero local dipole moments are evaluated by representing the corresponding s, p, s^*, and d orbitals in real space with Slater-type functions[30] and performing a numerical integration for the radial part and an exact integration for the angular part. The details of the calculation are given elsewhere.[31]

III. RESULTS AND DISCUSSION

A. Bulk InP

We first analyze the effect of hydrostatic pressure on the direct and indirect band gaps for bulk InP. This allows us to test the accuracy of our TB model for describing the evolu-

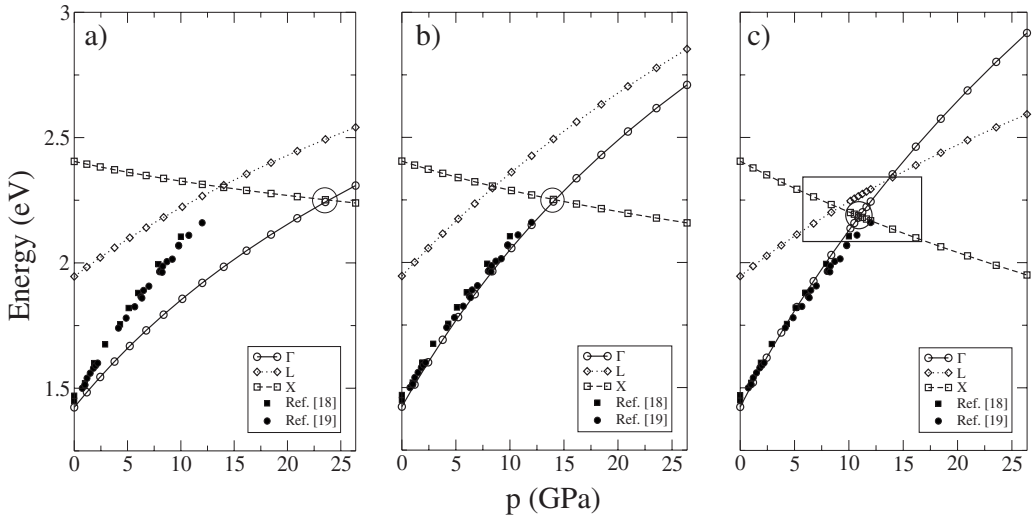

FIG. 2. Energy evolution with pressure for the lowest Γ_{1c} (solid line with dots), L_{1c} (dotted line with diamonds), and X_{1c} (dashed line with boxes) conduction-band minima with respect to the Γ_{1v} valence edge for bulk InP. Three different scaling laws have been used for the off-site TB parameters: (a) Harrison's scaling law, $\kappa=2.0$ (Refs. 32 and 33); (b) a single exponent, $\kappa=2.9$, determined by fitting the experimental band-gap volume deformation potential, $a_v^{\Gamma_c\text{-}\Gamma_v}=-5.68$ eV (Ref. 34); and (c) scaling laws of Jancu *et al.* for the different off-site TB parameters (Ref. 17). For sake of comparison, the experimental band-gap transition energies for values up to 10.8 GPa are included. Circles show the point where the Γ_{1c}-X_{1c} crossover takes place. The box in Fig. 1(c) marks the region where the Γ-X-L crossings appear.

tion of the lowest CB edges with pressure. In particular, the pressure where the Γ-X crossover takes place is determined and compared with experiment.[7] In Fig. 2, we evaluate the energy variation with pressure for the Γ_{1c} (circles), L_{1c} (diamonds), and X_{1c} (boxes) conduction-band edges with respect to the Γ_{1v} valence edge at the same pressure. We test three models for the scaling of the off-site TB parameters due to the lattice contraction: (a) Harrison's scaling law with $\kappa=2.0$ for all exponents,[32,33] (b) a single exponent, $\kappa=2.9$, determined by fitting the experimental band-gap volume deformation potential, $a_v^{\Gamma_c\text{-}\Gamma_v}$,[34] and (c) scaling laws of Jancu *et al.*, with different κ_{lm} for the different off-site TB parameters V_{lm}.[17]

In the absence of experimental information, Harrison's rule is often assumed to describe the effect of the variation in bond length on the TB parameters for strained systems.[24,35] The influence of the exponents κ_{lm} on the energy evolution with pressure for the lowest CB edges is examined in Fig. 2. For comparison, the experimental band-gap energies for pressures up to the crossover (10.8 GPa) are included.[18,19,36] Figure 2(a) shows that Harrison's rule does not provide a proper description of the Γ_{1c} energies with pressure. The predicted Γ-X crossing occurs at about $p=24$ GPa, which is more than twice the experimental value.[7]

In fact, simpler sp^3s^* models with Harrison's scaling law predict an erroneous positive pressure coefficient at the X_{1c} edge, rather than the correct negative coefficient.[17] This failure arises because the corresponding wave function in the vicinity of X_{1c} contains a large contribution from d states which have a bonding character. The $sp^3d^5s^*$ TB model ensures the correct sign for the X-gap pressure coefficient regardless of the scaling law employed, as observed in Fig. 2.

For a given TB parametrization, the corresponding scaling law for a hopping integral can be derived by calculating the dependence of the energy bands on volume. That procedure was followed in Fig. 2(b) only for the Γ_{1c}-Γ_{1v} transition. Although the evolution of the Γ_{1c} edge with pressure follows the experimental data, the Γ-X crossing ($p\simeq 14$ GPa) is overestimated. This is a consequence of the fact that volume effects have only been evaluated at the Γ point, which does not ensure the correct quantitative evolution of the different CB minimum with pressure.

In the $sp^3d^5s^*$ parametrization that we employ here, different scaling laws for different TB parameters were derived empirically by modeling to deformation potentials of band positions at Γ, X, and L. As a result, not only is the pressure dependence for the Γ_{1c} minimum correctly reproduced [Fig. 2(c)], but the pressure dependence for the band-edge points X_{1c} and L_{1c} is reproduced too. The linear pressure dependence for the X gap of InP, $\frac{dE_X}{dp}$, was determined experimentally in Ref. 7, $\frac{dE_X}{dp}=-17\pm3$ meV/GPa. Our theoretical results predict a bowing in the X_{1c}-edge energy versus pressure [Fig. 2(c)] so the energy dependence departs from linearity. However, if we fit the X_{1c} edge in the 0–15 GPa range (region where the Γ-X crossing takes place) to a linear dependence, then $\frac{dE_X}{dp}$ is -19 meV/GPa, in good agreement with experiment. Figure 2(c) shows that the Γ_{1c}-X_{1c} crossover takes place at the same lattice contraction as in the experiment, $\frac{\Delta a}{a_0}=0.037$,[7] which corresponds to a pressure of 10.9 GPa from Murnaghan's equation with the bulk modulus values of Ref. 3 (11.2 GPa if we employ the bulk modulus values of Ref. 5). The correct description of the lowest CB minimum with pressure ensures that the agreement between the theoretical and the experimental crossover pressure is not fortuitous. Therefore, scaling laws of Jancu *et al.* will be employed to study the InP nanocrystals.

Pseudopotential theory[5] and the Wannier function method[20] have also been employed to study the Γ-X crossing. Both methods predict the Γ-X crossover to occur at larger lattice contractions, $\frac{\Delta a}{a_0}$, than in the experiment. Pseudopoten-

tial theory $\left(\frac{\Delta a}{a_0}=0.0414\right)$[5] and the Wannier function method $\left(\frac{\Delta a}{a_0}=0.0420\right)$[20] overestimate the experimental lattice contraction $\left(\frac{\Delta a}{a_0}=0.0370\right)$ by more than 10%. Another significant difference between our model and these previous theoretical calculations is the energy evolution of the L_{1c} minimum. We find the energy difference between the Γ_{1c} and L_{1c} edges at the crossing point to be about 80 meV, significantly lower than the energy separation ($\simeq$0.3 eV) predicted by the Wannier method.[20] The value of the Γ_{1c}-L_{1c} separation is important because the existence of a Γ_{1c}-L_{1c} crossing near the Γ_{1c}-X_{1c} crossover has been proposed in Ref. 12 to explain the bowing in the band-gap variation against pressure for small nanocrystals. The proximity of the L_{1c} and Γ_{1c} edges in our TB model causes the Γ-L crossover to appear at low pressures ($p \simeq 14$ GPa) for the bulk InP crystal, close to the Γ_{1c}-X_{1c} crossover, and suggests that the L_{1c} minimum may play a role in the description of the band-gap variation with pressure for confined systems.

In previous calculations,[5,20] a local-density approximation (LDA) bulk band structure was taken as reference. Since LDA is well known to underestimate the bulk band gap, a rigid shift of the conduction band was performed to match the experimental zero-pressure band gap.[20] This shift took into account only the Γ_{1v}-Γ_{1c} separation. As a result, the indirect band gap Γ_{1v}-L_{1c} at zero pressure was significantly overestimated. LDA predicts the Γ-L band-gap separation to be over 0.75 eV, in contrast to the experimental value which is below 0.6 eV.[37] The differences between our model and previous calculations are further enhanced since the pressure dependence for the L gap is lower in our TB model (we obtain a linear dependence of 28 meV/GPa in the [0,16] GPa range). According to the Wannier method, the Γ-L crossing does not even occur at the investigated experimental pressures.[20] In the following, we will analyze in detail the role of the L_{1c}-derived states in the direct-to-indirect crossover for small nanocrystals.

B. InP nanocrystals

Atomistic calculations predict that direct-to-indirect transitions for nanocrystals should occur at reduced pressures relative to the bulk transitions. This occurs because confinement reduces the X_{1c}-Γ_{1c} and L_{1c}-Γ_{1c} separations. This confinement effect was investigated experimentally in Ref. 12. For quantum dots with average diameters $\langle D \rangle$ of 32 and 35 Å, the band-gap downturn occurs between 6.5 and 7.0 GPa, a much lower pressure than that in the bulk. This downturn was attributed to the existence of a Γ_{1c}-X_{1c} crossover that possibly occurs with an additional crossover with the L band at intermediate pressure. At pressures below the downturn, a bowing in the PL emission vs pressure curve was observed. To justify the sublinear behavior for the band-gap dependence on pressure, two different mechanisms were proposed. In the first one, a pure Γ-X transition was considered. To fit the PL emission curve, a large mixing potential for the Γ_{1c} and X_{1c} energy levels was derived, $V_{\Gamma X}=70$ meV. Such interaction is considerably larger than the interaction predicted theoretically in the framework of pseudopotential theory, $V_{\Gamma X} \simeq 2$ meV,[5] and lowers the band gap near atmospheric pressure below the measured value. These inconsistencies led the authors in Ref. 12 to suggest that the direct-to-indirect behavior could be explained as a sequence of Γ-L and L-X crossings. Reasonable intervalley potentials, $V_{\Gamma L}$ and V_{LX}, arise from this assumption.[12] However, neither pseudopotential theory[5] nor the Wannier function method[20] predicts the existence of a Γ-L crossing before the Γ-X crossover. An L-X crossing can occur at lower pressures compared to the Γ-X crossover. However, as shown in Figs. 2 and 3, the L-X crossing occurs at higher energy and does not distort the band gap.

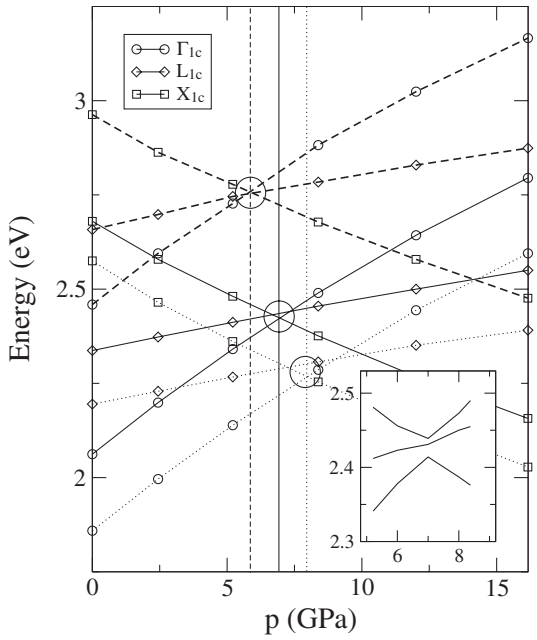

FIG. 3. Energies of the lowest Γ_{1c}- (circles), L_{1c}- (diamonds), and X_{1c}- (boxes) derived states versus pressure for InP nanocrystals of diameter D equal to $4a_0$, i.e., 23 Å (dashed line), $6a_0$, i.e., 35 Å (solid line), and $8a_0$, i.e., 47 Å (dotted line) for the bond-length-scaling model. Circles mark the crossing points. Vertical lines indicate the pressure at which the Γ_{1c}-X_{1c} crossover occurs. The inset shows these energy levels in the vicinity of the crossing point for the 35 Å dot.

1. Emission spectra: The bond-length-scaling TB model

In this paper, we analyze the evolution of the lowest Γ_{1c}-, L_{1c}-, and X_{1c}-derived states with pressure to determine the mechanism of the downturn observed experimentally. We first consider the model with a simple scaling of the bond lengths in the whole nanocrystal to describe the pressure effects. The conduction energies found with this model are shown in Fig. 3 for nanocrystals of diameters $D=4a_0$ (dashed line), $D=6a_0$ (solid line), and $D=8a_0$ (dotted line), where a_0 is the bulk lattice constant at zero pressure applied. The corresponding dot sizes are 23, 35, and 47 Å, respectively. The inset shows the energy levels of the 35 Å dot in the vicinity of the downturn point in more detail. From Figs. 2 and 3, we see that in the scaling model the nanocrystal states follow bulk states as a function of pressure. Thus, as obtained previously with pseudopotential theory[5] and the

TABLE I. Orbital contribution to the ground electron state, e_1, at $p=6$ and 8 GPa, as calculated by the scaling TB model. Coefficients for projection on the In and P states at the bulk minima: Γ_{1c}, L_{1c}, and X_{1c} are also shown to identify the bulklike nature of the nanocrystal state.

	$s(a)$	$p(a)$	$d(a)$	$s^*(a)$	$s(c)$	$p(c)$	$d(c)$	$s^*(c)$
Γ_{1c}	41.3	0.0	0.0	15.4	41.3	0.0	0.0	2.0
L_{1c}	14.5	13.9	8.0	6.2	28.6	25.8	3.0	0.0
X_{1c}	3.2	0.0	28.4	4.6	0.0	50.3	13.5	0.0
e_1 ($p=6$ GPa)	34.3	6.8	1.2	15.3	32.6	6.6	1.1	2.1
e_1 ($p=8$ GPa)	3.9	1.5	28.4	4.6	1.0	45.7	14.8	0.1

Wannier function method,[20] confinement energies[38] are nearly pressure independent. The energy variation with pressure, $\frac{dE}{dp}$, is enough to identify the bulk minima from which these states arise. Orbital contributions can also be employed to establish the bulk-band nature of a nanocrystal state. The lowest Γ_{1c}, L_{1c}, and X_{1c} bulk minima exhibit different orbital contributions (shown in Table I) which allows us to determine the bulk-band minima from which a particular state arises. This analysis is particularly useful for deciding the character of a given state in the vicinity of a crossing point.

In agreement with previous theoretical calculations, the scaling TB model predicts a size-dependent Γ_{1c}-X_{1c} crossover. The indirect-gap behavior is observed at pressures of $\approx$6, $\approx$7, and $\approx$8 GPa, for the nanocrystal sizes corresponding to 23, 35, and 47 Å, respectively. In particular, the transition pressure for the 35 Å dot matches the experimental value.[12] To test the accuracy of the scaling TB model for describing the optical properties of InP nanocrystals under pressure, we compare in Fig. 4 the band-gap dependence on pressure for a nanocrystal of diameter $6a_0$ ($D=35$ Å) with

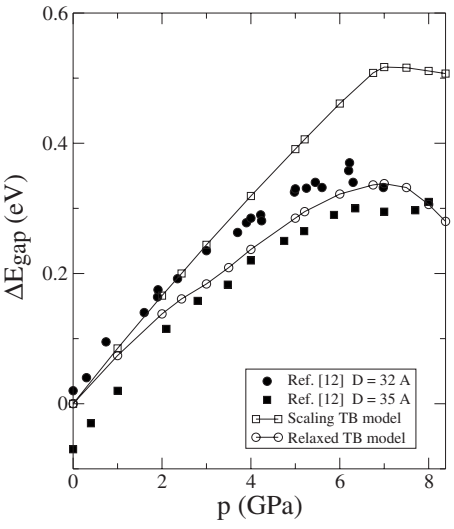

FIG. 4. Band-gap variation with pressure predicted by the bond-length-scaling model (solid line with open boxes) and the lattice-relaxed TB model (solid line with open circles) for a 35 Å dot. Our theoretical results are compared with the experimental results obtained in Ref. 12 for nanocrystals with average sizes of 32 Å (full dots) and 35 Å (full boxes).

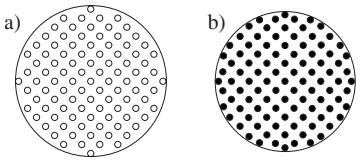

FIG. 5. Atom positions in the $z=0$ plane for a 47 Å dot under a 16 GPa hydrostatic pressure according to (a) the bond-length-scaling model and (b) the lattice-relaxed TB model.

the PL emission peak evolution of dot ensembles with average diameters $\langle D\rangle=32$ and 35 Å. According to the scaling TB model, the band gap varies linearly at a rate of 75 meV/GPa up to $p=7$ GPa, where the Γ_{1c}-X_{1c} crossover occurs. Such a pressure rate variation describes reasonably well the band-gap evolution at low pressure (up to 2 GPa) but not the bowing at larger pressures. As a result, the band-gap shift at the crossing point is overestimated, as seen in Fig. 4. The scaling TB calculations predict a Γ-L crossing at high pressure (see Fig. 3), which does not reduce the band gap at low pressures. In particular, for dot sizes between 32 and 35 Å, no Γ_{1c}-L_{1c} crossing is observed at about $\approx$3 GPa, as suggested in Ref. 12. For those and smaller nanocrystal sizes, all three bulk-band-derived states (Γ_{1c}, X_{1c}, and L_{1c}) are mixed at the crossing point (see inset of Fig. 3), and it becomes impossible to establish the nature of the ground electron state according to the orbital contributions. However, at pressures slightly above and below the downturn CB X_{1c} and Γ_{1c} states, respectively, are the ground state.

The linear band-gap response obtained with the bond-length-scaling model in the framework of the pseudopotential approach,[5] the Wannier function method,[20] and tight-binding theory (present work) cannot explain quantitatively the evolution of the experimental emission with pressure (Fig. 4). This suggests that a model with homogeneous scaling of the bond distances is too crude to describe pressure effects on nanocrystals.

2. Emission spectra: The lattice-relaxed TB model

For this reason, we have developed a more realistic model in which the strain energy for a dot under hydrostatic pressure is minimized. In Fig. 5, we compare the atom positions on the $z=0$ plane for a nanocrystal of diameter $8a$ under a large pressure of 16 GPa as described by (a) the bond-length-scaling model and (b) the lattice-relaxed TB model. The average bond length in the lattice-relaxed nanocrystal corresponds to the bond length in the scaling model. In particular, the atom in the center of the lattice-relaxed dot exhibits this mean bond distance value (see Fig. 6). Similarly, only small bond-angle variations with respect to the ideal tetrahedral angle are observed at the dot center. However, both the bond angle and bond distance distributions become wider away from the dot center. This broadening results from the rearrangement of the atoms in the dot to occupy more efficiently a spherical volume. The differences in the atom distributions for the faceted dot modeled by scaling the bond distance and the dot where the lattice relaxation effects have been included are evident from Figs. 5(a) and 5(b).

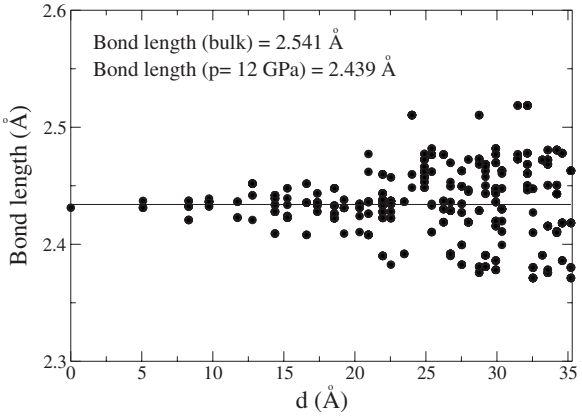

FIG. 6. Bond-length distribution obtained in the lattice-relaxed model versus distance from the dot center of a 35 Å diameter nanocrystal under a hydrostatic pressure of 12 GPa. The average bond length inside the dot is the same as the bond length assumed in the scaling model (solid line) and corresponds to the bond length obtained in the dot center.

The band-gap evolution with pressure predicted by the lattice-relaxed model is in agreement with the experimental results (see the solid line with dots in Fig. 4). In particular, the experimental bowing of the band-gap curve that was not accounted for by previous scaling models is now well described. To understand the different behavior predicted by the two TB models, we analyze separately the ground electron and hole energies as a function of pressure (see Fig. 7). In the scaling model, the ground electron energy changes at a uniform rate of 52 meV/GPa until $p=7$ GPa, where the Γ_{1c}-X_{1c} crossing occurs. No change in the Γ_{1c}-derived S-type electron ground-state wave function [see Fig. 8(a)] is observed in this pressure range. For higher pressures, a sixfold degenerate[39] state made of X_{1c} bulk states becomes the ground electron state [see Fig. 8(b)]. The corresponding ground electron charge density distributions above and below the downturn are very similar [compare Figs. 8(a) and 8(b)]. The larger effective mass at the X_{1c} edge leads to a larger charge density concentration in the dot center, as compared with the Γ-derived state. Despite the similarity of the states, it is straightforward to determine the bulk-band minima that define the states by looking at the orbital contribution. In Table I, we list the orbital contribution for the ground electron state at $p=6$ GPa and $p=8$ GPa obtained from the simple scaling model and compare them with the orbital contributions at the Γ_{1c}, X_{1c}, and L_{1c} bulk minima. We find no significant mixture between the different bulk-band minima in the vicinity of the crossing point. By projecting the ground electron state at $p=6$ and $p=8$ GPa onto the first 50 electron dot states at zero pressure, we get contributions larger than 95% from the corresponding S states arising from the Γ_{1c} and X_{1c} bulk-band minima, respectively. Significant mixture of the bulk-band minima is found only at the crossing point. The mixing potential $V_{\Gamma LX}$ (Ref. 40) between all three CB edges is $V_{\Gamma LX}=9$ meV for the 35 Å dot.

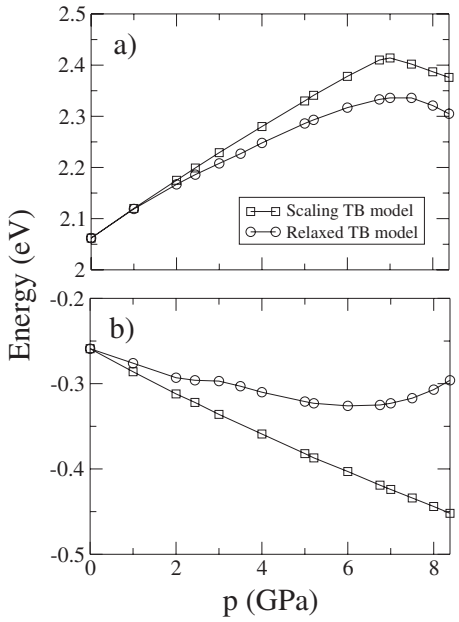

FIG. 7. Evolution with pressure of the ground-state energy for (a) electron and (b) hole states predicted by the bond-length-scaling model (solid line with boxes) and the lattice-relaxed TB approach (solid line with dots) for a 35 Å dot.

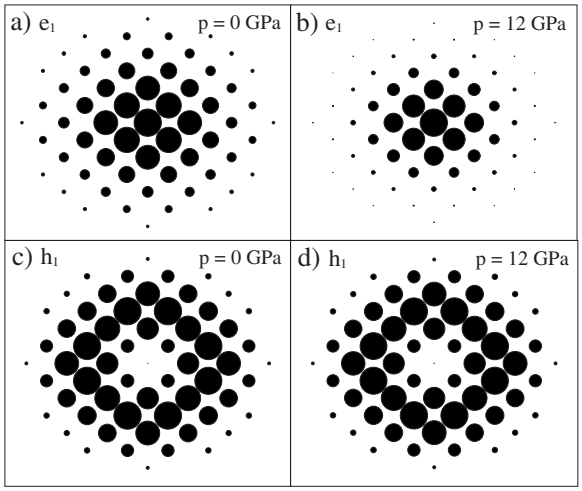

FIG. 8. Charge density calculated with the bond-length-scaling model for (a) the ground electron state at $p=0$ GPa, (b) the ground electron state at $p=12$ GPa, (c) the ground hole state at $p=0$ GPa, and (d) the ground hole state at $p=12$ GPa. The size of the dots quantifies the charge density on anions in the dot midplane.

In contrast to the scaling model, the ground electron energy in the lattice-relaxed model has a nonlinear dependence on pressure. At low pressures (0–2 GPa), the energy variation is similar to the scaling model, but the linear coefficient decreases to 40 meV/GPa in the 2–6 GPa range. The bowing of the curve is due to the strong mixing between the Γ_{1c}- and L_{1c}-derived states. For $p=3$ GPa, the contribution of the L_{1c} minima to the ground electron state is over 10% and increases monotonically with pressure (41% at $p=7$ GPa). At the crossover pressure ($p=7.5$ GPa), the L_{1c} contribution reaches its maximum, and the Γ_{1c} contribution, which was dominant at lower pressures, becomes negligible (below 5%), i.e., a Γ_{1c}-L_{1c} crossover takes place. The crossing is not sharp like the transitions predicted by the scaling model, but

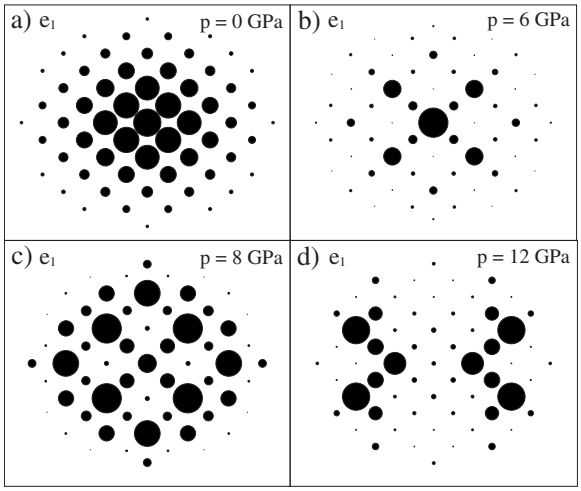

FIG. 9. Charge density in the $z=0$ plane for the ground electron state calculated with the lattice-relaxed TB model at (a) $p=0$ GPa, (b) $p=6$ GPa, (c) $p=8$ GPa, and (d) $p=12$ GPa.

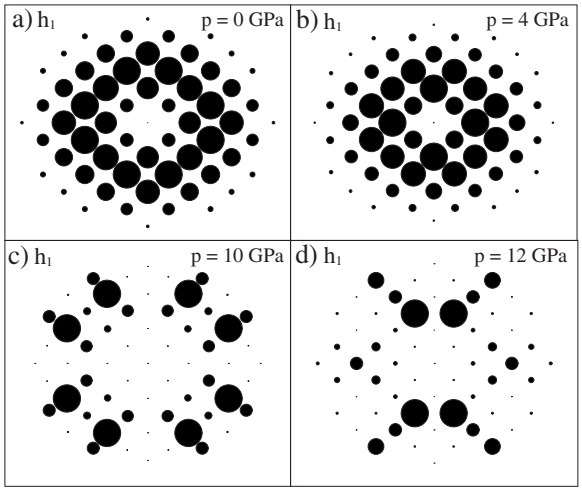

FIG. 10. Charge density in the $z=0$ plane for the ground hole state calculated with the lattice-relaxed TB model at (a) $p=0$ GPa, (b) $p=4$ GPa, (c) $p=10$ GPa, and (d) $p=12$ GPa.

rather is an increasing mixture extended over a large pressure range. The Γ_{1c}-L_{1c} mixing is responsible for the sublinear behavior observed experimentally. As a result of this mixture, the charge density for the ground electron state becomes more localized in the dot center [compare Figs. 9(a) and 9(b)].

For larger pressures, the ground electron energy decreases in the lattice-relaxed model. This energy decrease is accompanied by an increase of the X_{1c} component (from 6% at $p=7$ GPa to 30% at $p=10$ GPa). However, the main component remains L_{1c}-like, decreasing from 69% at $p=7.5$ GPa to 50% at $p=10$ GPa. For pressures greater than 7 GPa, the ground electron state cannot be completely described by projecting its wave function onto the first Γ_{1c}, X_{1c}, and L_{1c} electron states for zero pressure applied. The missing contribution results from the increasing surface localized character of these states at high pressures. The lattice-relaxed model predicts a correlation between the shortening of the average bond length near the dot center as a function of pressure and the increase in the distribution of bond lengths and bond angles near the dot surface. After the crossover, charge density localization to the outer part of the dot becomes dominant [see Fig. 9(c)]. For higher pressures ($p=12$ GPa), a band of electron surface states with energies in the band gap is formed.[41]

The differences between the two TB models are greater for hole levels. The bond-length-scaling model predicts that the hole energy monotonically decreases (i.e., moves further below the band edge) as a function of pressure [Fig. 7(b)]. However, the lattice-relaxed model predicts a more complex behavior for hole states. In the bond-length-scaling model, the ground hole state energy changes linearly at a rate of 23 meV/GPa. Little change in the charge distribution of the hole states is observed at high pressure. In particular, the envelope function of the ground hole state, which exhibits a P symmetry, is the same for the whole pressure range studied [compare Figs. 8(c) and 8(d)]. In contrast, according to the lattice-relaxed model, the ground hole state decreases its energy only up to $p=6$ GPa. The energy dependence on pressure is less pronounced than in the simple scaling model, and a kink in the energy curve versus pressure is observed. The kink appears in the energy region where the maximum of the charge density is squeezed from a distance of $2a$ to a distance of $1a$ with respect to the dot center.[42] Increasing pressure leads to a slightly stronger localization near the dot center. In fact, the ground hole charge density distribution is very similar to the charge density presented in Fig. 10(b) even well after the downturn ($p=8$ GPa). For larger pressures, localization effects dominate and the charge distribution changes radically, as shown in Fig. 10(c). As with electron states, at high pressures ($p=12$ GPa) hole states form a band of surface states with energies in the band gap [see Fig. 10(d)].

3. Experiments of Lee et al.: Downturn at bulklike pressures

The band-gap dependence on lattice contraction, $\frac{\Delta a}{a_0}$, was also studied by photoluminescence and fluorescence line narrowing (FLN) for 27 and 37 Å diameter nanocrystals in Ref. 13. Contrary to the experiments in Ref. 12 that we have discussed so far, little reduction in the downturn pressure with respect to the bulk crossover pressure is observed in the investigated nanocrystals of Ref. 13. The reasons for this bulklike behavior in nanocrystals are not well understood. In the following, we will analyze the effect of size, geometry, and partial passivation in the framework of the lattice-relaxed and scaling models to check if any of the above experimental uncertainties can justify the observation of the downturn at bulklike pressures.

In Fig. 11(a), we compare the band-gap variation versus lattice contraction as calculated by the bond-length-scaling model for three different nanocrystals of diameters $D=23$, 35, and 47 Å with the experimental results obtained in Ref. 13. The band-gap variation changes linearly with lattice contraction, but with slopes of different signs before and after the Γ_{1c}-X_{1c} crossover predicted by the scaling model. A simple extrapolation of these two linear dependences for each nanocrystal size yields the downturns indicative of the

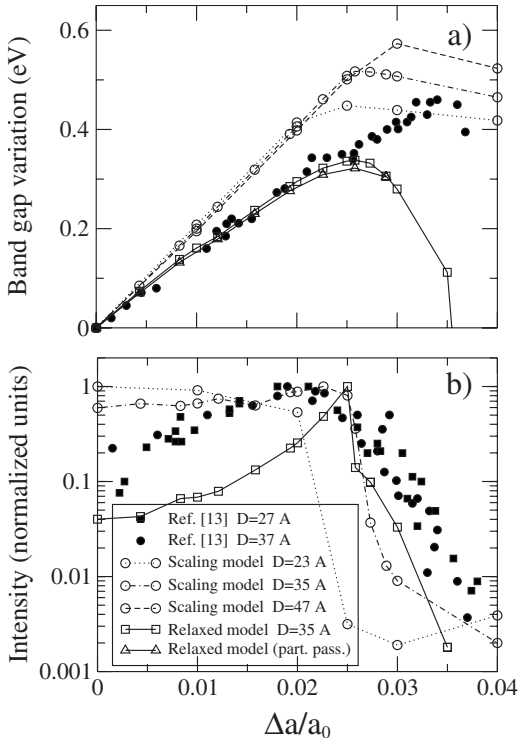

FIG. 11. (a) Band-gap variation versus lattice contraction predicted by the scaling TB model for spherical nanocrystals of diameter $D=23$ Å (dotted line with circles), $D=35$ Å (dot-dashed line with circles), and $D=47$ Å (dashed line with circles) compared to the results arising from the lattice-relaxed TB model for a 35 Å dot (solid line with boxes). The effect of partial passivation on surface atoms has also been studied in the framework of the lattice-relaxed model (solid line with triangles). (b) Intensity of the ground transition calculated with the scaling model for a 23 Å dot (dotted line with circles) and a 35 Å dot (dot-dashed line with circles). The results obtained with the lattice-relaxed model for a 35 Å dot are also shown (solid line with boxes). Our theoretical results are compared with the PL emission energies and intensities obtained in Ref. 13 for nanocrystals with mean diameters $D=27$ Å (full boxes) and 37 Å (full dots).

indirect-band-gap behavior. Similar to the experiment, the downturns are sharper for larger nanocrystals and reach larger values of the band-gap variation. We note that the band-gap variation with pressure predicted by the scaling model is size independent in the region where the band gap is direct. According to the scaling TB model, the band gap increases by about 0.2 eV per $0.01\frac{\Delta a}{a_0}$ before the Γ_{1c}-X_{1c} crossing takes place. Such an increase is larger than the band-gap variation with $\frac{\Delta a}{a_0}$ measured in the experiment ($\simeq 0.15$ eV per $0.01\frac{\Delta a}{a_0}$) for the 37 Å dots, as shown in Fig. 11(a). Moreover, the experimental downturns appear at higher pressures than in the scaling TB model and seem less dependent on nanocrystal size.

It is not clear why in the PL experiments of Ref. 13 the downturns appear at high pressures similar to the pressures observed for the bulk transition. To better understand possible reasons for this behavior, we have studied the role of the geometrical distortions from the spherical shape. Geometry is a source of uncertainty since the synthesized nanocrystals employed in Ref. 13 were found to be slightly ellipsoidal with an aspect ratio varying between 1 and 1.15.[21] We consider elliptical nanocrystals with an aspect ratio equal to 1.15. No significant change of the band-gap evolution with lattice contraction is observed for such ellipticity. The ellipsoidal dots investigated here experience downturns at the same pressures as the spherical dots. In fact, the near-band-edge optical structure of the ellipsoids is very similar to the optical structure of the spherical dots, the only significant difference being the lifting of the degeneracies.

The lattice-relaxed model [solid line with boxes in Fig. 11(a)] predicts a band-gap evolution with lattice contraction at low pressures in agreement with the experimental results obtained in Ref. 13 [black dots in Fig. 11(a)]. However, as described previously, the predicted band-gap downturn appears at $p=7$ GPa $\left(\frac{\Delta a}{a_0}=0.26\right)$, well below the experimental downturn at $\frac{\Delta a}{a_0}=0.35$.

X-ray photoelectron spectroscopy (XPS) was used in Ref. 21 to measure the elemental composition of the nanocrystals employed in Ref. 13 and to determine the coverage of the trioctylphosphine oxide (TOPO) capping group. XPS measurements concluded that the synthesized nanocrystals were close to stoichiometric InP and exhibited TOPO coverages below 50% for nanocrystal sizes between 27 and 37 Å. Thus, not only the P sites but also some In sites remain unpassivated.[43] The band-gap energies at atmospheric pressure for the 27 and 37 Å nanocrystals studied in Ref. 13 are below 1.95 and 2.1 eV, respectively. Larger band gaps, in agreement with our theoretical TB results, have been measured for the same nanocrystal sizes (see, e.g., black box results in Fig. 3 of Ref. 20). The lower band gaps measured experimentally in Ref. 13 can be attributed to the role of partial passivation. Thus, the effect of nanocrystal passivation has been investigated to determine if partial passivation can account for the large downturn pressures measured in the samples of Ref. 13. We have modeled the effects of partial passivation on surface atoms by assuming a smaller potential shift of either the cation or the anion dangling bonds or of all the surface dangling bonds. The external dangling bond potential is chosen to reproduce the zero-pressure experimental band gaps obtained in Ref. 13. The same dangling bond potential is then used for higher pressures. For this choice of dangling bond potential, the surface states due to dangling bonds remain outside of the band gap.

Our calculations which include lattice relaxation show that the evolution with pressure of the lowest energy transitions involving the Γ_{1c}, L_{1c}, and X_{1c} electron states is not significantly altered by the description of the surface for any of the passivation models studied. This is shown in Fig. 11(a), where the band-gap variation for a 35 Å dot with all surface dangling bonds partially passivated (solid line with triangles) is compared with that for the fully passivated dot and the experimental results. In both cases, the band gap varies for increasing pressure with the same slope.

In partially passivated nanocrystals, the splitting between the Γ_{1c}-derived electron states and the X_{1c}- and L_{1c}-like states is enhanced due to increased level repulsion between the Γ_{1c}-derived electron states and the dangling bond surface states outside the gap. This effect is a direct consequence of

the different effective masses at the various bulk-band minima. The lower Γ-point effective mass gives rise to more extended states which are more sensitive to the description of the surface. Due to the increased band splitting, the Γ_{1c}-X_{1c} *crossover* pressure can be dependent on the nanocrystal surface passivation even though the *slope* of the pressure dependence of the band gap is found to be insensitive to the passivation model. This dependence of the crossover pressure on band splitting is more important for the TB scaling model. For partially passivated nanocrystals, like those described before, the Γ_{1c}-X_{1c} crossover occurs at pressure values around $p=10$ GPa $\left(\frac{\Delta_a}{a_0}=0.35\right)$ in the scaling model, in the region where the experimental downturns occur. However, the energy variation with pressure of the direct-gap transitions (i.e., below the crossover point) is unaffected by the passivation model. Thus, the scaling model still predicts a band-gap increase with pressure (i.e., the slope) which is too large, even for partial passivation. The effect of partial passivation is less significant in the lattice relaxation model because the crossover is determined by the pressure where states localize and is less sensitive to the band splittings that determine when states cross.

According to the lattice-relaxed model, localization effects on the dot exterior instead of the Γ_{1c}-X_{1c} crossover are responsible for the downturns observed experimentally. Since the localization of the charge density is due to the broad distribution of bond angles and distances in the outer part of the dot, the downturn pressure predicted by the lattice-relaxed model is not altered by the passivation of the surface, as shown in Fig. 11(a) (solid line with triangles). However, a possible explanation for the observation of the downturn at higher pressures arises from the surface localization of the lowest energy states, which might have reduced their contribution to the experimental spectra. In the following, we analyze in detail the nature of the emission state studied in Ref. 13 to assess this hypothesis.

We compare the emission intensity obtained experimentally[13] with the results of the bond-length-scaling and lattice-relaxed TB models. Interestingly, the experimental drop in intensity in Ref. 13 occurs at $p=5.7$ GPa $\left(\frac{\Delta a}{a_0}=0.22\right)$, well before the measured redshift at about $p=10$ GPa $\left(\frac{\Delta a}{a_0}=0.35\right)$. The scaling model predicts that the Γ_{1c}-X_{1c} crossover is accompanied by a sharp (3 orders of magnitude) decay in the oscillator strength. Since the Γ_{1c}-X_{1c} crossover is size dependent, the decay appears at lower pressures as size decreases. In Fig. 11(b), we show the emission intensity for a 35 Å dot (dashed-dotted line with circles) and for a 23 Å dot (dotted line with circles) predicted by the scaling TB model. Their intensities decay sharply at $\frac{\Delta a}{a_0}=0.025$ and $\frac{\Delta a}{a_0}=0.020$, respectively. In contrast, the experimental band-gap luminescence intensity for the 27 Å (full boxes) and for the 37 Å (full dots) nanocrystals are very similar and exhibit their maxima at the same lattice contraction [see Fig. 11(b)]. The experimental emission data also show an enhancement of 1 order of magnitude for increasing pressure up to $p=5.7$ GPa. Simple scaling models do not predict such an enhancement since both electron and hole envelope wave functions remain unaffected in the whole direct-gap region.

A different scenario is obtained in the lattice-relaxed model. Both electron and hole wave functions concentrate in the dot interior before the downturn pressure at $p=7$ GPa. The oscillator strength increases 1 order of magnitude before the downturn, as is shown in Fig. 11(b) (solid line with boxes) for the 35 Å dots. This enhancement in the oscillator strength suggests an increased overlap between the electron and hole wave functions. The oscillator strength reaches its maximum at the downturn point and decays by 3 orders of magnitude as a result of the localization to the surface. A similar decay after the downturn is seen for smaller (23 Å diameter) dots and for larger (46 Å diameter) dots in the lattice-relaxed model. However, before the downturn pressure, there is a size dependence to the increase of the intensity with pressure. For large dots, there is little variation in the intensity with pressure before the downturn. For small dots, the intensity increases for increasing pressure up to the transition pressure. However, the increase is not as dramatic as for 35 Å dots. This suggests that how the electron and hole states localize toward the dot center as the pressure increases up to the transition pressure is determined in part by the dot size. Because the pressure dependence of the intensity is dependent on dot size, the good qualitative agreement between theory and experiment for the specific dot sizes studied experimentally further confirms that the lattice-relaxed model provides a good description of the pressure effects and is a better model than the bond-length-scaling description. For pressures above 7 GPa, the lattice-relaxed model predicts the existence of localization effects, yielding weak transitions that show a larger Stokes shift from the first absorption peak.[44] However, if we trace the evolution of the first absorption peak instead of the emission peak, the downturn pressure moves to higher values $\left(\frac{\Delta a}{a_0}\simeq 0.30\right)$. Since in Ref. 13 PL and FLN techniques were employed to measure the emission peak, we suggest that the lowest energy states might have been missed in the experimental analysis due to their surface localization. This would lead to the observation of the late downturns reported in Ref. 13.

To check the predictions arising from the lattice-relaxed model and, therefore, confirm the mechanism responsible for the downturns observed experimentally, it would be valuable to know the band-gap evolution after the downturn. According to the lattice-relaxed model, the formation of both electron and hole surface localized states yields a sharp decay in the band-gap variation with pressure after the downturn, while the existence of transitions to X_{1c}-derived electron states is consistent with a slowly varying band gap over a large pressure range after the downturn. In Fig. 11(a), the experimental band-gap variation for pressures only below 11 GPa is shown. However, the authors in Ref. 13 state that at 12.3 GPa, trap emission dominates the photoluminescence, which is consistent with the scenario described by the lattice-relaxed model.

4. Absorption spectra

To complete our analysis of the optical properties of InP nanocrystals under pressure, the near-band-edge optical spectra for quantum dots with different sizes ($D=4a_0$, $6a_0$, and $8a_0$) and geometries (spheres and ellipsoids) have been investigated at different pressures. In Fig. 12, we have considered a nanocrystal with diameter $6a_0$ ($D=35$ Å), similar

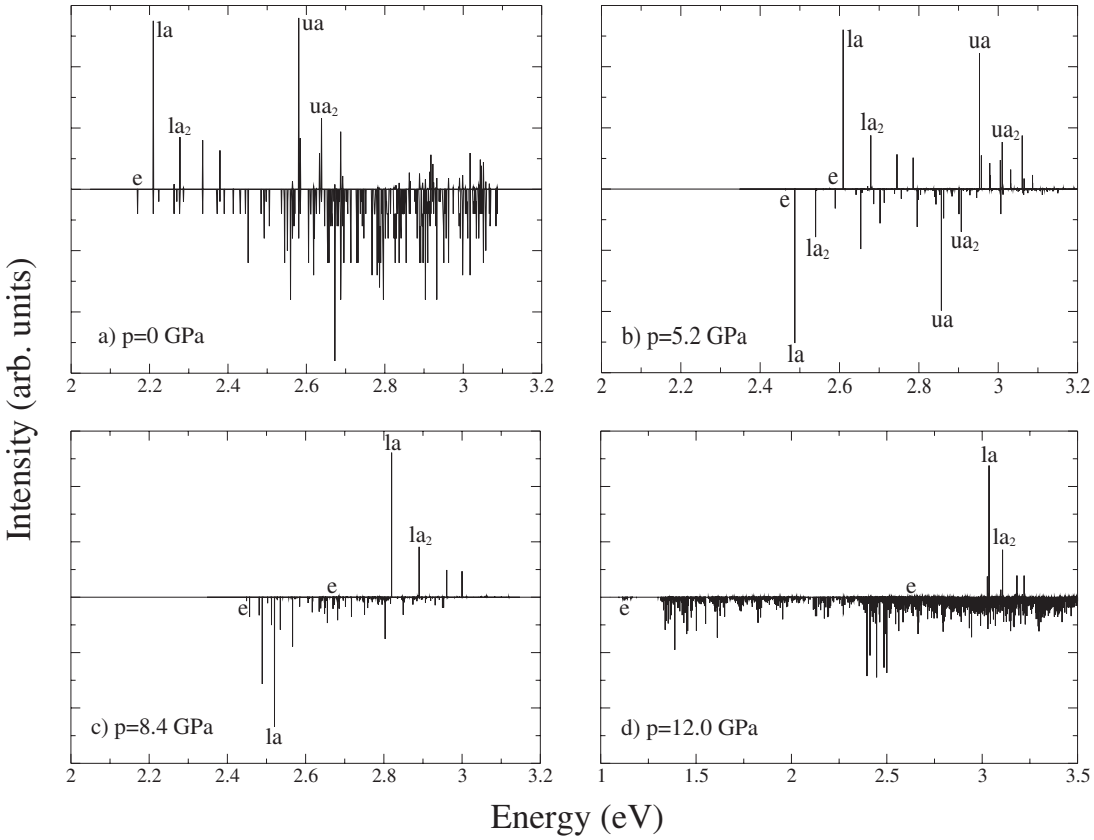

FIG. 12. Near-band-edge optical spectra for a 35 Å dot calculated with the scaling TB model (upper part of the panels) and the lattice-relaxed TB model (lower part of the panels). Different pressures (p=0, 5.2, 8.4, and 12.0 GPa) have been investigated in panels (a)–(d). In (a), we plot the optical spectrum at atmospheric pressure (upper part). In the lower part of panel (a), we include the density of transitions. Main absorption transitions (la, ua, la_2, and ua_2) and the emission peak (e) are labeled in the spectra. The oscillator strength for p=12.0 GPa in the lattice-relaxed model has been multiplied by 10 to make it visible in the spectrum.

to those investigated in Refs. 12 and 13, and studied its optical spectrum at four different pressures (p=0, 5.2, 8.4, and 12.0 GPa), corresponding to the four distinct pressure regimes: atmospheric pressure, immediately before the downturn, immediately after the downturn, and well above the downturn. The upper part of the panels in Fig. 12 shows the spectra predicted by the bond-length-scaling model. In the lower part, we plot the spectra resulting from the lattice-relaxed model. Figure 12(a) corresponds to the spectrum at atmospheric pressure. In the lower part of Fig. 12(a), we include the density of transition to show the different electron-hole pairs for which we have evaluated the oscillator strength.

The main optical transitions (la, la_2, ua, and ua_2) have been labeled in the spectra. Without exception, those intense peaks correspond to direct $\Gamma_{1c} \leftarrow \Gamma_{1v}$ transitions. In particular, the la and la_2 transitions involve the ground electron state with, respectively, the first hole state of S symmetry (la) and the corresponding split-off partner (la_2). The first excited electron state, which has P symmetry, is involved both in the ua transition (with the ground hole state at zero pressure applied) and the ua_2 transition (with the lowest split-off hole level of P symmetry). The position of the emission peak, e, is also shown in the spectra.

For pressures below the downturn [p=5.2 GPa spectra in Fig. 12(b)], the whole near-band-edge optical spectra are blueshifted. Both the lattice-relaxed and simple scaling models predict the same structure, the only difference being the smaller blueshift arising from the lattice-relaxed model, as discussed previously. In particular, the energy separation between the main absorption peaks ($ua-la$, la_2-la, and ua_2-ua splittings) is maintained. No significant differences are found for ellipsoids with a similar number of atoms.

After the downturn, the differences between the two models are more significant. The bond-length-scaling model predicts a linear increase of the Stokes shift, i.e., the energy difference between the lowest absorbing (la) and emitting (e) states. This behavior is a consequence of the different nature of the emitting state before and after the downturn. Before the downturn, the emission peak consists of a direct transition between the ground electron state (S symmetry) and the ground hole state (P symmetry). The ground transition is orbital forbidden and dim; consequently, it is active only in emission. Before the crossover, the energy difference with respect to the first absorption peak (la) remains small (below 40 meV for nanocrystals with $D \geq 6a_0$) and pressure independent. After the downturn, the emission peak involves a X_{1c}-derived electron state. The ground transition is now dark since it is indirect in the reciprocal space. Indirect transitions to the X_{1c}- and L_{1c}-derived states calculated in the framework of the scaling model are typically 2 or 3 orders of magnitude less intense than the dim ground transition ob-

served before the downturn. In contrast, the lowest absorption peak (*la*) always involves the Γ-derived electron and hole states of *S* symmetry regardless of the pressure applied. Because the L_{1c}- and, particularly, the X_{1c}-derived electron levels become more stabilized with respect to the Γ_{1c}-derived states with increasing pressure and yield weak transitions, larger differences are found between the lowest absorption and emission peaks as pressure increases, i.e., a larger Stokes shift.

The spectra predicted by the lattice-relaxed model are more complex. The downturn coincides with a direct-to-indirect transition too, but instead of the pure Γ_{1c}-X_{1c} crossover predicted by the scaling model, we observe a predominant L_{1c} character for the ground electron state immediately after the downturn, i.e., a Γ-*L* crossover. As pressure increases, the X_{1c} bulk minima become more important in the description of the lowest electron states. Those electron states with a significant Γ_{1c} character may give rise to transitions with a large oscillator strength. This is the case for the transition labeled as *la* in Fig. 12(c). However, the main effect after the downturn is the increasingly localized character of both electron and hole states to the outer part of the dot. For larger pressures [$p=12$ GPa in Fig. 12(d) (Ref. 45)], those localized states yield surface-band transitions with energies in the band gap. As a result, optical properties are dominated by trap emission and the fine structure observed at low pressures is suppressed.

IV. SUMMARY

We have employed an $sp^3s^*d^5$ tight-binding model to study the optical properties of InP crystals under pressure. In particular, the pressure-induced direct-to-indirect band gap transition has been analyzed in detail for the bulk and small InP nanocrystals. Our TB model with *d* orbitals accurately describes the evolution of the lowest conduction-band edges with pressure and predicts the bulk Γ_{1c}-X_{1c} crossover to occur at the same pressure as in the experiment.

To describe the optical properties of InP nanocrystals under pressure, two different models have been proposed. In the scaling model, the bond lengths are assumed to change homogeneously in the whole nanocrystal as a function of pressure. This model predicts confinement energies that are nearly pressure independent and overestimates the band-gap variation with pressure. The experimental redshift is explained as a Γ_{1c}-X_{1c} transition which occurs at lower pressures compared to that in the bulk.

In the lattice-relaxed model, the strain energy for a nanocrystal compressed in a given volume is minimized. The relaxation of the lattice yields new atomic positions where bond angles as well as bond lengths vary in the nanocrystal. The band-gap evolution with pressure predicted by this model is in agreement with the photoluminescence emission experiments performed in Refs. 12 and 13. This is a consequence of the increasing mixture of the L_{1c} and X_{1c} bulk minima with pressure and the more localized character of hole states. The predicted downturn agrees well with the experimental results of Ref. 12. The downturn coincides with a Γ_{1c}-L_{1c} crossover for the electron states, but is mainly due to the localized character of both electron and hole states. The role of size, geometry, and surface passivation has been analyzed in detail within the two tight-binding models to justify the late downturns measured in Ref. 13. The nature of the emission state has been monitored by studying its oscillator strength as a function of pressure.

Our results show that the optical fine structure predicted by the two tight-binding models before the downturn is the same. After the downturn, the differences between the two models are greater. In the simple scaling model, direct $\Gamma_{1c} \leftarrow \Gamma_{1v}$ transitions are shifted to higher energies, leading to a linear increase of the Stokes shift with pressure. In contrast, localization effects predicted by the lattice-relaxed model lead to the formation of surface-band transitions with energies in the band gap. As a result, the optical structure observed at low pressures is completely suppressed.

ACKNOWLEDGMENTS

This work was performed under the sponsorship of the U.S. Department of Commerce, NIST, and was also supported by Polish Projects Nos. 3T1104326 and PZB-MIN-008/P03/2003.

*garnett.bryant@nist.gov

†Present address: Institute for Microstructural Sciences, National Research Council of Canada, 1200 Montreal Road, Ottawa, Ontario K1A 0R6, Canada.

[1] J. R. Chelikowsky, Phys. Rev. B **35**, 1174 (1987).
[2] R. K. Singh and S. Singh, Phys. Rev. B **39**, 671 (1989).
[3] C. S. Menoni and I. L. Spain, Phys. Rev. B **35**, 7520 (1987).
[4] Y. K. Vohra, S. T. Weir, and A. L. Ruoff, Phys. Rev. B **31**, 7344 (1985).
[5] H. Fu and A. Zunger, Phys. Rev. Lett. **80**, 5397 (1998).
[6] A. R. Goni, K. Strössner, K. Syassen, and M. Cardona, Phys. Rev. B **36**, 1581 (1987).
[7] S. Ernst, A. R. Goni, K. Syassen, and M. Cardona, Phys. Rev. B **53**, 1287 (1996).
[8] M. A. Malik, M. Afzaal, P. O'Brien, U. Bangert, and B. Hamilton, Mat. Sci. Technol. **20**, 959 (2004).
[9] J. G. Díaz and G. W. Bryant, Phys. Rev. B **73**, 075329 (2006).
[10] H. Fu and A. Zunger, Phys. Rev. B **56**, 1496 (1997).
[11] S. H. Tolbert, A. B. Herhold, L. E. Brus, and A. P. Alivisatos, Phys. Rev. Lett. **76**, 4384 (1996).
[12] C. S. Menoni, L. Miao, D. Patel, O. I. Micic, and A. J. Nozik, Phys. Rev. Lett. **84**, 4168 (2000).
[13] C.-J. Lee, A. Mizel, U. Banin, M. L. Cohen, and A. P. Alivisatos, J. Chem. Phys. **113**, 2016 (2000).
[14] J. G. Díaz, W. Jaskólski, M. Zieliński, and G. W. Bryant, Phys. Status Solidi C **3**, 3832 (2006).
[15] J. G. Díaz, G. W. Bryant, and W. Jaskólski, Phys. Status Solidi C **3**, 3823 (2006).

[16] J. G. Díaz, M. Zieliński, W. Jaskólski, and G. W. Bryant, Phys. Rev. B **74**, 205309 (2006).
[17] J.-M. Jancu, R. Scholz, F. Beltram, and F. Bassani, Phys. Rev. B **57**, 6493 (1998).
[18] H. Müller, R. Trommer, M. Cardona, and P. Vogl, Phys. Rev. B **21**, 4879 (1980).
[19] C. S. Menoni, H. D. Hochheimer, and I. L. Spain, Phys. Rev. B **33**, 5896 (1986).
[20] A. Mizel and M. L. Cohen, Solid State Commun. **113**, 189 (2000).
[21] A. A. Guzelian, J. E. B. Katari, A. V. Kadavanich, U. Banin, K. Hamad, E. Juban, A. P. Alivisatos, R. H. Wolters, C. C. Arnold, and J. R. Heath, J. Phys. Chem. **100**, 7212 (1996).
[22] O. I. Micic, C. J. Curtis, K. M. Jones, J. R. Sprague, and A. J. Nozik, J. Phys. Chem. **98**, 4966 (1994).
[23] G. W. Bryant and W. Jaskólski, J. Phys. Chem. B **109**, 19650 (2005).
[24] K. Leung and K. B. Whaley, J. Chem. Phys. **110**, 11012 (1999).
[25] S. Pokrant and K. B. Whaley, Eur. Phys. J. D **6**, 255 (1999).
[26] F. D. Murnaghan, Proc. Natl. Acad. Sci. U.S.A. **30**, 244 (1944).
[27] The cut-off radius is a distance slightly smaller than the spherical radius. The cut-off radius ensures a faster convergence of the minimization process.
[28] W. H. Press, B. P. Flannery, S. A. Teukolski, and W. T. Vetterling, *Numerical Recipes* (Cambridge University Press, Cambridge, 1986).
[29] J. C. Slater and G. F. Koster, Phys. Rev. **94**, 1498 (1954).
[30] J. C. Slater, Phys. Rev. **36**, 57 (1930).
[31] S. Lee, J. Kim, L. Jönsson, J. W. Wilkins, G. W. Bryant, and G. Klimeck, Phys. Rev. B **66**, 235307 (2002).
[32] W. A. Harrison, Phys. Rev. B **8**, 4487 (1973); W. A. Harrison and S. Ciraci, *ibid.* **10**, 1516 (1974); S. T. Pantelides and W. A. Harrison, *ibid.* **11**, 3006 (1975).
[33] W. A. Harrison, *Electronic Structure and the Properties of Solids* (Freeman, San Francisco, 1980).
[34] The volume deformation potential $a_v^{\Gamma_c\text{-}\Gamma_v}$ was derived from the pressure coefficient, $a_p^{\Gamma_c\text{-}\Gamma_v}=8.0$ meV/kbar (Ref. 37) via the relationship $a_v^{\Gamma_c\text{-}\Gamma_v}=B_0 a_p^{\Gamma_c\text{-}\Gamma_v}$, where B_0 is the bulk modulus.
[35] S. Schulz and G. Czycholl, Phys. Rev. B **72**, 165317 (2005).
[36] No experimental data for pressures above 10.8 GPa are available because the band-gap evolution with pressure is obscured by a phase transition from zinc blende to rocksalt structures.
[37] *Semiconductors. Intrinsic Properties of Group IV Elements and III-V, II-VI, and I-VII Compounds*, edited by O. Madelung, Landolt-Börnstein New Series, Group III, Vol. 22, Pt. A (Springer, Berlin, 1987).
[38] The confinement energy $\Delta\varepsilon_\gamma(p)$ is defined as the energy difference between the nanocrystal energy and the bulk energy at a given pressure: $\Delta\varepsilon_\gamma(p)=\varepsilon_\gamma^{dot}(p)-\varepsilon_\gamma^{bulk}(p)$.
[39] Spin-orbit coupling lifts the ideal sixfold degeneracy into a twofold and a fourfold degenerate state that are very close in energy (less than 5 meV). The charge density state shown in Fig. 8(b) is made of all six energy levels.
[40] The anticrossing gap, i.e., the smallest energy difference between the anticrossing curves in Fig. 3, gives the effective Γ-L-X mixing potential, $V_{\Gamma LX}$.
[41] As can be observed in Figs. 9(d) and 10(d), at very high pressures some symmetries of the dot states appear to be removed. In part, this occurs because only the $z=0$ plane is shown. Three-dimensional plots are more symmetrical. Moreover, after states localize at the surface, the states have a higher degeneracy. One particular state is shown in the figures.
[42] The envelope P symmetry of the ground hole state prevents the charge density from being concentrated in the dot center.
[43] In and P surface atoms exhibit very different coordination properties. While the In atoms act as a Lewis acid, the P sites behave as a Lewis base. The donor character of TOPO explains its preferential coordination to the In sites.
[44] Below 7 GPa, the first absorption peak is near the emission peak. The differences between the two peaks are under 40 meV in the 0–7 GPa range.
[45] The optical spectrum of Fig. 12(d) has been calculated considering both the first 200 electron and hole states, instead of the first 50 states as it was done in previous cases, to cover the same energy range investigated at low pressures.